NASA TECHNICAL MEMORANDUM NASA-TM-75377 19790010743 ASA TM-75377

VORTEX PATTERN DEVELOPING ON THE UPPER SURFACE OF A SWEPT WING AT HIGH ANGLE OF ATTACK

J. Mirande, V. Schmitt, and H. Werlé

Translation of "Système Tourbillonnaire Présent à l'Estrados d'Une Aile en Flèche à Grande Incidence," Office National d'Etudes et de Recherches Aerospatiales (ONERA), Chatillon, France, Report ONERA TP-1978-124, October 4-6, 1978, 18 pages

NATIONAL AERONAUTICS AND SPACE ADMINISTRATION
WASHINGTON, D.C. 20546 MARCH 1979

STANDARD TITLE PAGE

1. Report No.	2. Government Accession No.	3. Recipient's Catalog No.
NASA TM-75377		

4. Title and Subtitle	5. Report Date
VORTEX PATTERN DEVELOPING ON THE UPPER SURFACE OF A SWEPT WING AT HIGH ANGLE OF ATTACK	March 1979
	6. Performing Organization Code

7. Author(s)	8. Performing Organization Report No.
J. Mirande, V. Schmitt and H. Werle ONERA	10. Work Unit No.

9. Performing Organization Name and Address	11. Contract or Grant No.
Leo Kanner Associates, Redwood City, California 94063	NASw-3199
	13. Type of Report and Period Covered

12. Sponsoring Agency Name and Address	14. Sponsoring Agency Code
National Aeronautics and Space Administration, Washington, D.C. 20546	

15. Supplementary Notes

Office National d'Etudes et de Recherches Aerospatiales (ONERA), Chatillon, France, Report ONERA TP 1978-124

16. Abstract In view of the ever greater interest shown for flying at high angle of attack, it deems necessary to further investigate the flows that, though separated from the wing, remain organized as stable vortex sheets, thus conditioning handling qualities and performance of combat aircraft. To this end, an experimental study, based on a swept wing, has been undertaken in the water tunnel and the wind tunnel at low speeds (V_o 90 m/s), with a view to improve our understanding of the intervening phenomena and to make easier their modelling.

The vortex flow effects on the wing are first illustrated from global effort measurements and static pressure distributions. We deduce the domain of existence of this type of flow, as a function of both sweep angle and angle of attack. By a phenomenological study in the water tunnel, we then attempt to describe the physical pattern of the vortex flow, from its formation near the apex to its breakdown at the trailing edge. Lastly, we determine, by means of a clinometric probe, the flow field over the wing.

17. Key Words (Selected by Author(s))	18. Distribution Statement
	Unclassified - Unlimited

19. Security Classif. (of this report)	20. Security Classif. (of this page)	21. No. of Pages	22. Price
Unclassified	Unclassified		

VORTEX PATTERN DEVELOPING ON THE UPPER SURFACE OF A SWEPT WING AT HIGH ANGLE OF ATTACK

J. Mirande, V. Schmitt, and H. Werlé
Office National d'Etudes et de Recherches Aerospatiales (ONERA)

1. Introduction

The performance and handling qualities of combat aircraft/1* at high angle of attack depend greatly on the degree of organization of the separations appearing on such configurations. Visualizations realized in a water tunnel on a model of a variable-geometry aircraft (Fig. 1) show, by way of example, a disorganized separation on the upper wing (Fig. 1 a b b') or a breakdown of vortex flow on the upper surface (Fig. 1 c d d') capable of causing undesirable effects on the performance and handling qualities.

Thus, it is essential to know the structure of flows of this type separated from the wing as well as the factors which control the phenomena of formation and destruction of coherent vortex flows. These are the reasons and objectives of this basic study made by the ONERA in both wind and water tunnels. It is based on the AFV-D wing having variable sweep angles, the experimentation on this wing falling within the more general category of research related to anything from three-dimensional flows to transonic speeds [1].

2. Vortex Flows Over Wings With Variable Sweep Angles /2

2.1. Testing Techniques and Conditions

The AFV-D wing with variable sweep is a rectangular wing having a "peaky" symmetrical ONERA'D' wing section (e/c 0.105) [2]. The sweepback is incorporated by rotation on an axis located near the socket (Fig. 2). In its design the wing undergoes

---

* Numbers in the margin indicated pagination in the foreign text.

a considerable variation in its aspect ratio as a function of the sweep angle which can be as large as $\phi = 60^\circ$.

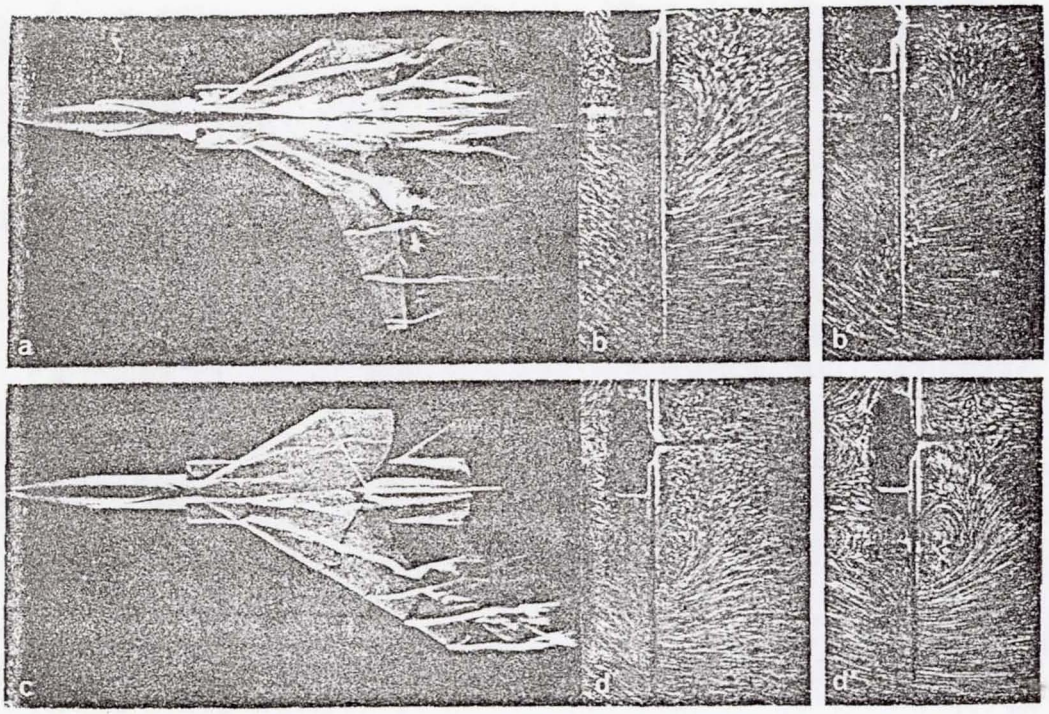

Fig. 1. - Flow around a model aircraft with variable sweep angle (water tunnel $Re_l \simeq 0.3 \times 10^4$)

a, c: views of the upper surface (dye visualization)
b, b', d, d': cross sections (air bubble visualization)
- above $\phi = 25^\circ$ } angle of attack $\phi = 10^\circ$ (a, b, c, d) and
- below $\phi = 60^\circ$ } 15° (b', d')

The main characteristics of the model used during the wind tunnel tests are given in Table 1 whereas the coordinates of section 'D' are specified in Table 2.

The tests were made in the ONERA S2Ch wind tunnel. It is an Eiffel closed-jet wind tunnel (diameter $\phi = 3$m), the maximum velocity of which is $V_o = 110$ m/s and the rate of turbulence is moderate ($\varepsilon = 0.003$). Since the wind tunnel is not pressurized, the range of the Reynolds number covered by velocity variation (40 m/s $< V_o < 90$ m/s) is relatively small ($0.8 \times 10^6 \leq Re_c \leq 1.9 \times 10^6$), c representing the chord line of the wing.

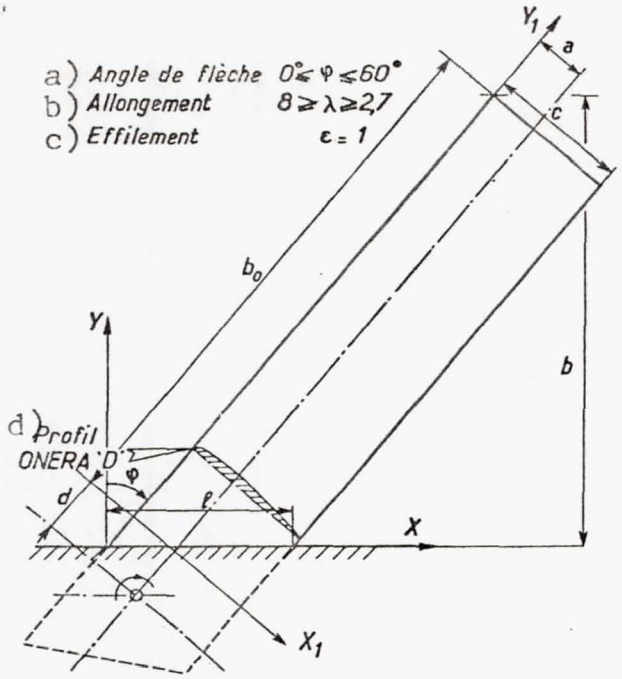

Key: a) Sweep angle, b) Aspect ratio, c) Streamlining, d) Section

Fig. 2. - Diagram of the AFV-D Wing with Variable Sweep

The model is mounted on the floor of the wind tunnel by means of a strut which ensures the angle of attack. A protective circular plate which is joined with the turret screens the wing from the effects of the boundary layer present on the wall of the wind tunnel.

Measurements are taken, first of all concerning the global forces and are determined by means of a six-component balance suspended from the wall. The measuring equipment for the model includes 341 static pressure gauges which are distributed in 11 sections of two. Due to the principle of design of this apparatus, the measurements are taken only at the rate of two sections per test by means of scanivalves.

The technique of visualizing flow lines along the wall is based on the use of a quasi-permanently fluid viscous coating. This coating is a mixture of liquid paraffin and titanium oxide. These visualizations, which are very useful in completing the information issuing from the measurements taken and in facilitating analysis, are not reversible due to the viscosity of the coating; thus precautions must be taken during their interpretation (see 4.2). /3 Moreover, a probing device has been developed for exploring the flow around the wing, and especially at the vortex structure level.

Figure 3 shows the model and the exploratory device allows a probe to be positioned in planes perpendicular to the root chord. It consists of a rail parallel to the chord which allows positioning at x and supports a vertical groove ensuring displacement along y of a slide consisting of a horizontal

TABLE I - GEOMETRIC CHARACTERISTICS OF THE AFV-D MODEL

$\varphi°$	l (m)	b (m)	λ	S_o (m^2)
0	0,300	1,200	8,00	0,3600
30	0,346	1,107	6,66	0,3573
40	0,392	1,002	5,66	0,3546
50	0,467	0,865	4,28	0,3500
60	0,600	0,700	2,87	0,3420

(a = 0.150 m and d = 0.060 m (Fig. 2))
ϕ : sweep angle; l : root chord;
b : semi-span; λ : aspect ratio;
S_o : wet surfact.

TABLE II- PROPORTIONS OF THE ONERA "D" SECTION

x_1/c	z_1/c	x_1/c	z_1/c
.000000	.000000	.072500	.035193
.000050	.001342	.077500	.035912
.000200	.002685	.082500	.036604
.000500	.004245	.087500	.037269
.001000	.006002	.092500	.037908
.001700	.007820	.105000	.039405
.002600	.009658	.120000	.041028
.003700	.011494	.135000	.042486
.005000	.013310	.155000	.044213
.006500	.015091	.195000	.047057
.008300	.016913	.235000	.049242
.010300	.018639	.275000	.050853
.012500	.020259	.315000	.051902
.015000	.021821	.355000	.052369
.017500	.023144	.395000	.052230
.020000	.024277	.435000	.051476
.022500	.025254	.475000	.050123
.025000	.026106	.520000	.047942
.027500	.026857	.580000	.044120
.030000	.027528	.640000	.039509
.032500	.028136	.690000	.035239
.035000	.028696	.730000	.031601
.037500	.029221	.770000	.027763
.040000	.029719	.810000	.023691
.042500	.030198	.850000	.019335
.045000	.030663	.890000	.014658
.047500	.031119	.930000	.009698
.052500	.032003	.970000	.004621
.057500	.032850	.990000	.002090
.062500	.033663	1.000000	.000780
.067500	.034444		

groove defining the displacements of axis z perpendicular to the plane of the wing.

The probe, a conical type with five taps, allows the vector velocity in modulus and direction to be determined with a precision varying from 1.5 to 5% in a range of angles from 0 to 30° . Beyond that, up to approximately 50°, the indications can be used qualitatively [3].

Besides the five pressures indicated by the probe, two distributions of parietal pressure (Fig. 3) were measured during the scannings to control the stability of the configuration and the extent of the effects of possible interaction of the probing apparatus.

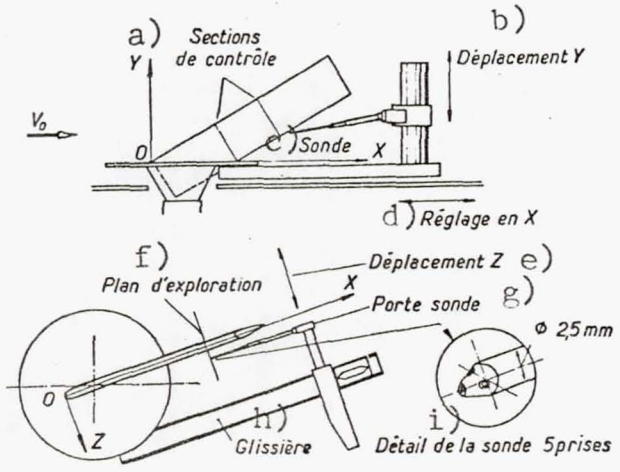

Fig. 3. The Mounted Apparatus
Key: a) Control sections, b) Y displacement, c) Probe, d) Adjustment along X, e) Z displacement, f)Exploration plane, g) Probe holder, h) Slide, i) The 5-pointed probe in detail

2.2. Formation and Effects of Vortex Flows

During the wind tunnel tests, the appearance of vortex flows is observed in a well-defined range of angle of attack and sweep angle.

Indeed, for sweep angles greater than or equal to $\phi = 40^\circ$ the lift curves indicate a very characteristic nonlinear path (See Fig. 4).

This behavior is the result /3 of the presence, on the upper surface of the wing, of a flow which is separated at the leading edge, but which becomes organized by forming a conical vortex which creates an appreciable gain in lift. The close study of

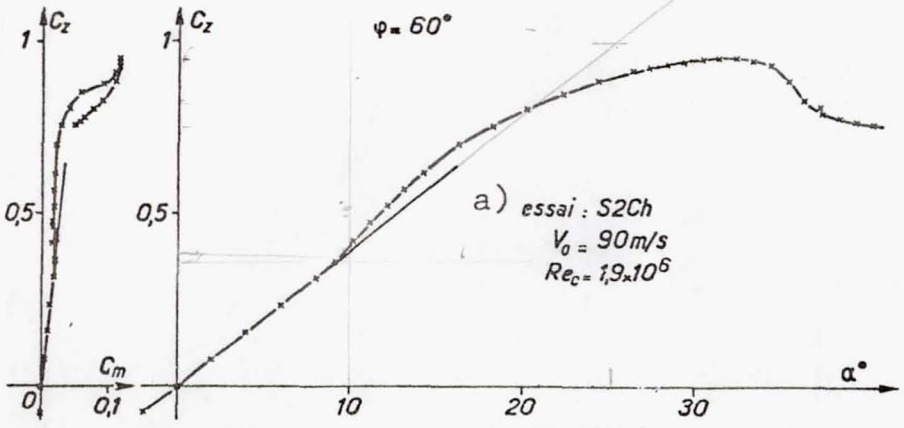

Fig. 4. - Lift and Pitching Moment
Key: a) test: S2Ch

this type of flow either in a water or wind tunnel by means of probings was made at a sweep angle of $\phi = 60$ which is a typical example.

Thus, we are presenting some characteristic results relative to this wing configuration. First of all, we will analyze the lift curves and pitching moment (Fig. 4) obtained with Reynolds number ($Re_c = 1.9 \times 10^6$). While the change in lift shows the characteristics indicated above, we will point out, in examining the pitching moment, a tendency of the wing to drop, when a vortex flow appears ($\alpha \approx 9°$) followed by an elevating divergence: this obviously indicates a change in the aerodynamic center resulting from the conical vortex whose position and intensity vary as a function of the angle of attack. Polars realized at an increasing then decreasing angle of attack generally result in curves which are not affected by hysteresis.

A more detailed study is possible by analyzing the field of static pressure on the upper surface of the wing. In order to reveal the change in phenomena as a function of the angle of attack, we examined the distribution of pressure in two sections

M = 0,27 ?

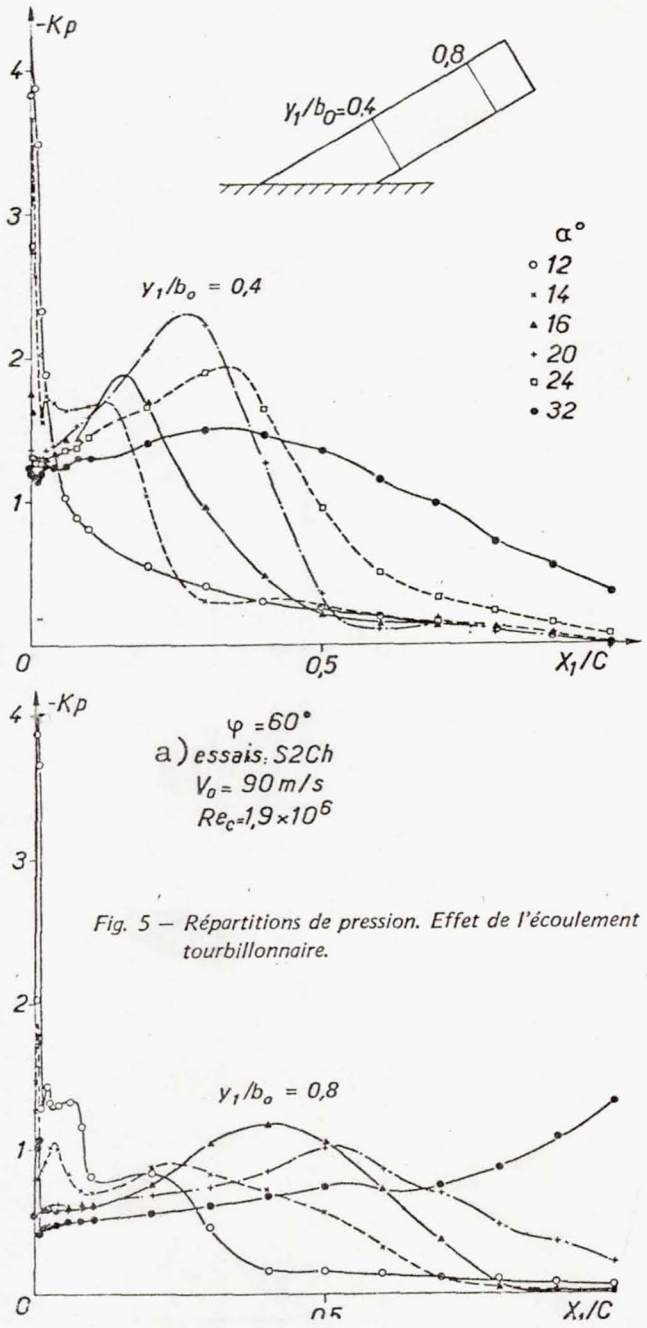

Fig. 5 — Répartitions de pression. Effet de l'écoulement tourbillonnaire.

Fig. 5. - Pressure distribution. Effect of vortex flow.
Key: a) tests

y_1/b_o = 0.4 and 0.8 (Fig. 5). The vortex system causes bell-shaped distributions which are more pronounced in the lower section than in the upper section. The maximum depressions (vortex kpmin), located at the level of the projection of the vortex axis in the wing plane (see 4.1 also), move towards the trailing edge when the angle of attack increases. A α =12° the pressure distribution in the section y_1/b_o = 0.4 characterized by a peak of overspeed at the leading edge followed by a continual recompression up to the trailing edge, corresponds to a still unseparated flow. The origin of the vortex which, according to the lift curve, nevertheless exists and must thus be located outside of the section y_1/b_o = 0.4. The flattening of the curves of the pressure coefficient at high angle of attack or even the disappearance of the vortex kpmin (for example, α = 32° at y_1/b_o=0.8) indicates the breakdown of the vortex whose intensity is increasingly reduced as the angle of attack increases. The joint examination of pressure distributions in all the sections and parietal visualizations discussed in detail later in this article allow it to be established that the position of the

vortex origin during time of its appearance is far from being located at the apex of the wing (Fig. 6a), but it tends towards that direction when the angle of attack increases. However, due to a lack of better measuring means, this origin cannot be precisely determined. As has already been said, figures for the vortex pressure coefficient kp_{min} lead to the approximate determination of the vortex axis projected in the wing plane. Thus, it is possible to schematically describe the changes of this axis which pivots slightly around the vortex origin towards the socket (Fig. 6b) when the angle of attack increases.

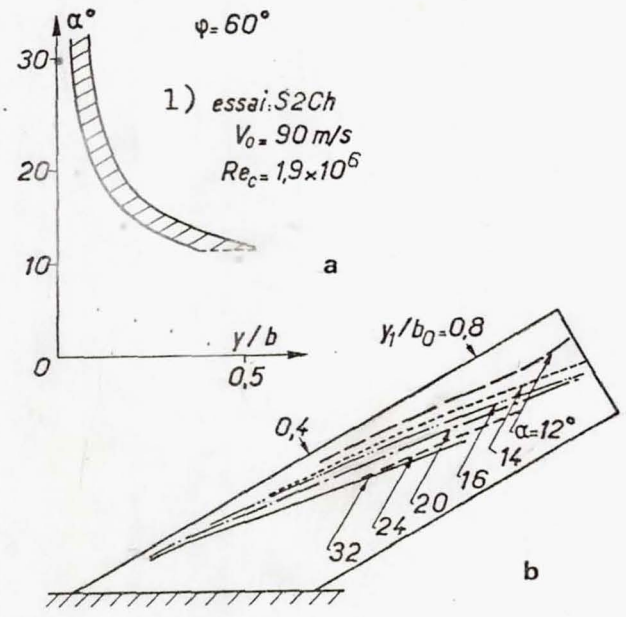

Fig. 6. - Vortex flow characteristics
a) path depending on the dimensions of the origin of the vortexes
b) approximate positions of the vortex axis as a function of the angle of attack
Key: 1) test, S2Ch

2.3. Effect of Reynolds Number /5

These tests also supplied some indications relative to the Reynolds number. An increase in the Reynolds number obtained by a velocity variation is indicated by a considerable reduction in the area of existence of vortex flows on the wing (Fig. 7). Their appearance in terms of the angle of attack is determined on this figure by a vortex value ΔC_z of approximately 0.02 taking into account the precision of the measurements. Let us note in passing that this appearance in wings with large sweep angles tends towards a value already observed[4] for stream-lined wings ($\alpha \approx 6°$). -The upper limit of the field is defined by the values $\alpha\ c_{z\ max}$ of the stall which corresponds to the premature breakdown of -the vortex. Lastly, the lateral limit of the field indicating

the minimum sweep for which this wing presents vortex flows is not exactly known, for the study of the sweep was made in steps of 5°.

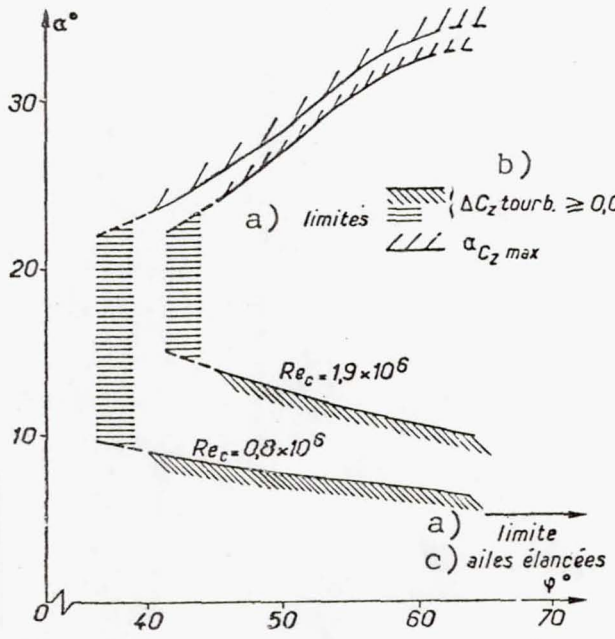

Fig. 7. - Field of existence of vortex flows.
Key: a) Boundaries, b) Vortex, c) Streamlined wings

The effect of the Reynolds number is again illustrated by the lift curves relating to the sweep $\phi=50°$ (Fig. 8). We note that the angle of attack of the appearance of the vortex flow increases appreciably whereas the maximum lift $c_{z\ max}$ and the corresponding angle of attack $\alpha_{cz\ max}$ decrease.

In order to shed more light on the profound transformation of the flow on the upper surface of the wing in terms of the Reynolds number, let us examine in detail what occurs with an angle of attack of $\alpha = 12$. According to the lift curves, the vortex flow is set up with Reynolds numbers $Re_c = 0.8 \times 10^6$ and 1.5×10^6, but a vortex effect is not evident with $Re_c = 1.9 \times 10^6$. This is confirmed by the pressure fields on the upper surface (Fig. 9). Indeed, the pressure distributions corresponding to the lowest Reynolds number ($Re_c = 1.3 \times 10^6$) indicate the presence of a vortex which is still not very intense. On the other hand, with a higher Reynolds number, the pressure distributions indicate an essentially nonseparated flow with a high overspeed peak at the leading edge and a recompression which continues to the trailing edge. The visualizations along the walls (Fig. 10) relative to the same configuration of the wing again corroborate this result. In the case of a small Reynolds number ($Re_c = 0.8 \times 10^6$) we observe lines of parietal

flow revealing a conical vortex by an inversion of the curve and characteristic single lines. On the other hand, in the case of higher Reynolds number (Re_c = 1.9 x 10^6), we especially note, besides a laminar separation bubble at the leading edge, a very pronounced secondary flow in the region of the trailing edge.

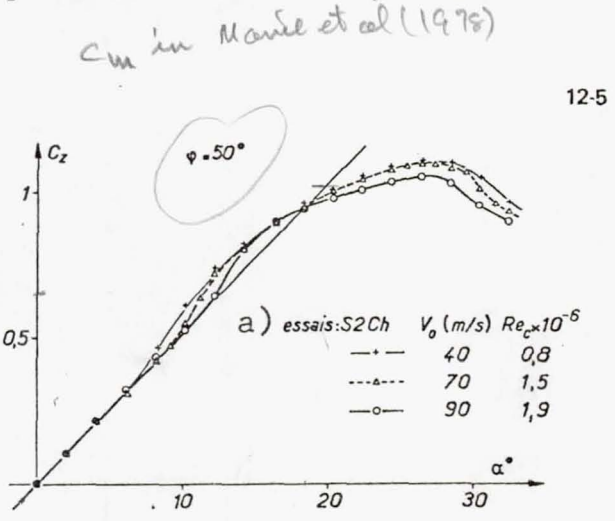

Fig. 8. - Influence of Reynolds Number on Lift
Key: a) tests

3. Phenomenological Study of Vortex Flow in a Water Tunnel With Low Reynolds Number /6

3.1. Experimental Conditions

This study used the vertical ONERA tunnel 5. The visualization processes by liquid or gas tracers, and especially their application to such separated flow studies[6] have been made known in numerous publications. The interested reader will find in these documents a complete explanation of the experimental technique used. Here we will limit our discussion to a succinct report of a few details necessary to the understanding of the results.

The dyes of the same density as the water were emitted from the surface of the models in the form of isolated filaments (for example Fig. 1a & c) or parietal sheets (for example Fig. 18 a-f) making visible in a stationary field, more or less outer parietal flow lines or surfaces according to the regulation of the dye output. In the moving or turbulent zones, an aleatory distribution and rapid diffusion of the dye emitted occurs, which then only reveals the average appearance of the phenomena.

The same is true for the gas tracers - miniscule air bubbles obtained when the tunnel is filled, whose trajectories in transversal

planes (for example Fig. 1 bb' dd') or longitudinal planes (for example, Fig. 17 a) are observed.

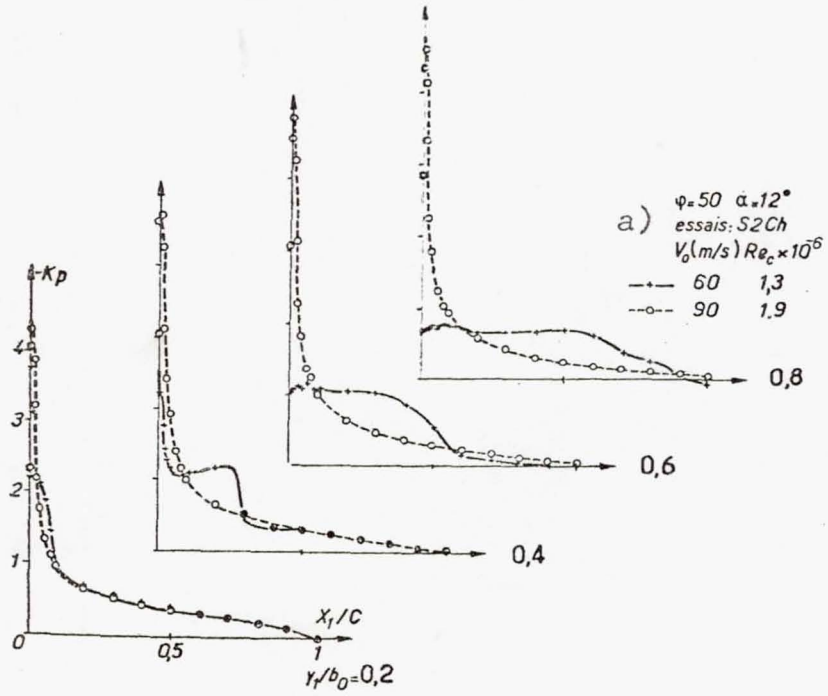

Fig. 9. - Static Pressure Fields on the Upper Surface. Effect of Reynolds Number
Key: a) tests

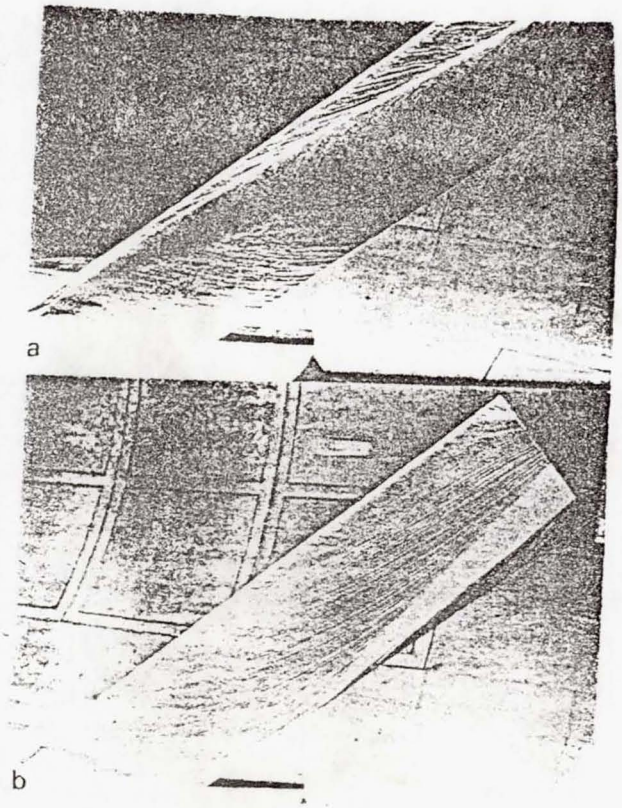

Let us observe here that these sections only give the appearance of the transverse pseudo-flow revealed by the trajectory elements of the air bubbles crossing the illumined section whose considerable thickness cannot and must not be too small (light necessary to expose negatives, length of the trajectory elements). But

Fig. 10 - Visualization of parietal flow lines. Effect of Reynolds number - Test S2Ch, ϕ = 50°, α = 12°.
a) V_o = 40 m/s; Re_c = 0.8 x 10^6
b) V_o = 90 m/s; Re_c = 1.0 x 10^6

this appearance especially depends on the orientation of the sighting axis (See Fig. 14). It is thus always necessary to carefully interpret the various air bubble visualizations by cross-checking them in particular with those obtained more directly by means of the dyes.

In order to make an analysis which is as precise as possible of the vortex structure of the upper surface separation near the apex and especially examine the interaction effects which are capable of occurring along the protective panel which supports the wings, we have used the enlarged model technique which represents, on a larger scale, the field in which one hopes to undertake a more detailed study. Of course, this procedure requires a comparison with a complete model.

All of the models tested in the tunnel are represented in Figure 11, which indicates in addition the position of the sections of transversal flow visualized by air bubbles. The geometric characteristics of the models (sweep $\phi = 60°$, ONERA'D' section) and the simulated Reynolds region are given in Table 3.

3.2. Structure of the Flow[12]

The visualizations obtained with the complete model (Fig. 12) provide the indispensable overall views of flow on which the stable vortex structure of separation on the upper surface and its path as a function of the angle of attack are distinguished.

At an angle of attack of 20° (Fig. 12 abb'), the sheet which unfurls along the swept leading edge twists into a "cone" [7, 8] around the main vortex of the upper surface issued near the apex. This vortex is situated diagonally above this nonconical wing and tends to breakdown downstream before the lower surface flow which passes around the free end of the model. Between the leading edge and this well structured vortex a marginal zone enclosed under the cone develops, which becomes disorganized downstream. This structure of the upper surface separation is confirmed by the appearance of the transversal pseudo-flow revealed

by the air bubbles (Fig. 12b).

When the angle of attack increases (Fig. 12 acd), we observe the progression upstream of marginal vortices, the development of the main vortex and the clear upward motion towards the apex of its breakdown point, a classical phenomenon 9 affecting all the vortex structures at high angles of attack.

A variation in the Reynolds number, such as might occur in the tunnels (see Table 3), causes no fundamental change in the appearance of the transversal pseudo-flow (compare Fig. 12 b and b'), Nor in the appearance of the breakdown (compare Fig. 12 c and c') On the other hand, at equal angles of attack, differences in origin and principal vortex position are recorded compared with those observed in the wind tunnel with high Reynolds number (Fig. 5 & 22).

Lastly, in order to complete this description, let us note the presence on the lower surface (Fig. 12e) of a departure line line which divides the part of the lower surface flow which flows onto the upper surface along the leading edge of the latter from that which returns to the trailing edge. The vortex sheet which becomes /7 separated along this accentuated swept edge also twists into a "cone" to form a concentrated vortex of the trailing edge, but which interacts considerably with the main vortex of the upper surface.

TABLE III - CHARACTERISTICS OF MODELS STUDIED IN THE WATER TUNNEL

Ref. fig.11	a) Modèle	c (mm)	b (mm)	λ	$Re_c \times 10^{-4}$
1	b) aile complète	50	109,5	2,7	0,25 - 1,0
2	c) aile agrandie	100	120	1,24	0,5 - 2,0
3	d) apex agrandi	100	100	1,33	0,5 - 5,0

Key:

a) Model
b) Complete wing
c) Enlarged wing
d) Enlarged apex

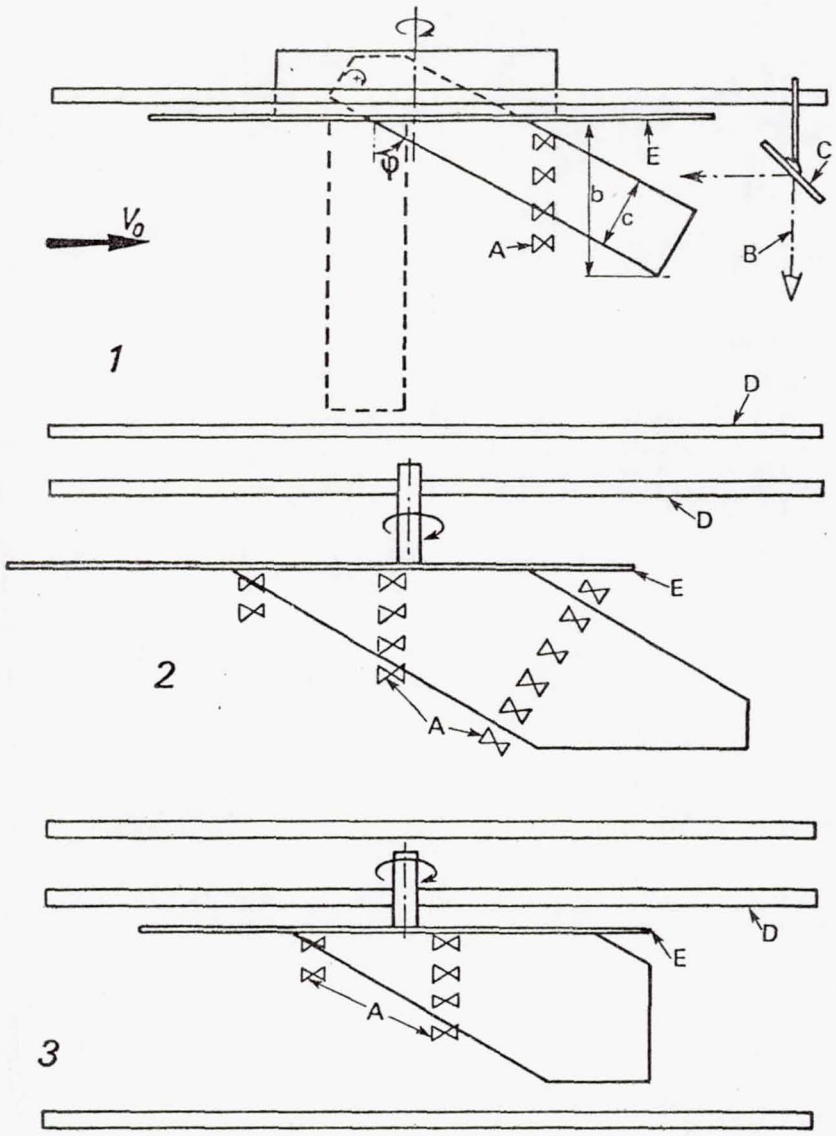

Fig. 11. - Diagrams of the models tested in the water tunnel ($\phi = 60°$)
A. cross-sections visualized by air bubbles,
B. corresponding axis of photograph taking,
C. mirror at 45° ,
D. wall of the jetstream (normal or reduced),
E. protective panel of the model.

The tests made at a 20° angle of attack with the enlarged /9 wing allowed the physical diagram of the flow to be studied thoroughly, especially thanks to the numerous dye emitters which are set up in this model (Fig. 13), as well as to the various cross-sections

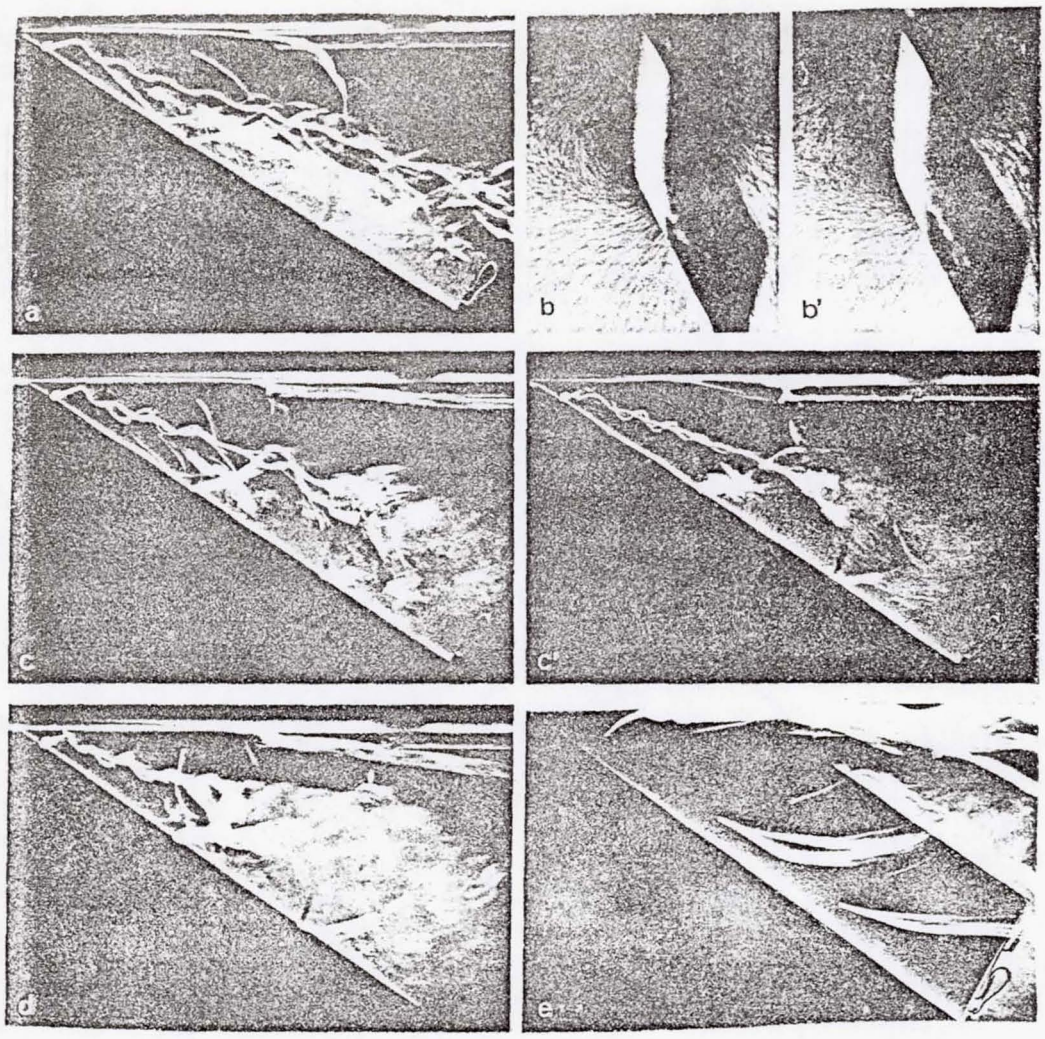

Fig. 12 - Flow around a model of a complete wing (water tunnel - $Re_c \simeq 0.5 \times 10^4$ except when indicated otherwise). Views of the upper surface (a, c, c', d) and of the lower surface (e) cross-sections (b, b')
- top $\alpha = 20°$
- middle $\alpha = 25°$ ($Re_c \simeq 10^4$ for b' and c')
- bottom $\alpha = 30°$.

/8

visualized by air bubbles (Fig. 14), which is possible to do with /9 such a model.

Under these conditions, the flow diagram which can be obtained from these tests at high angle of attack and low Reynolds number ($Re_c \approx 10^4$) is the following:

- the departure line P of the lower surface (Fig. 15a) originates from a single nonisotropic stagnation point located near the rounded apex of the model. Moving downstream, this boundary line, first of all oriented according to the bissector of the angle at the apex, curves in then and rapidly becomes parallel to the leading edge. From the stagnation point, which appears to be a point of retrogression, a second departure line becomes detached, curved in the opposite direction and which separates the flow on the lower surface which reunites with the trailing edge, from that which flows onto the protective panel due to the effect of a vortex which forms along the socket (Fig. 13a and 17 b);

- the separation line S on the upper surface (Fig. 15c) is also located on a generating line of the model, but in the immediate proximity of the leading edge, except near the apex where it curves in towards the socket (Fig. 13d). This incurvation of the departure and separation lines at the apex indicates a decrease in the local angle of attack accentuated by the effects of the boundary layer of the protective panel;

- indeed, the boundary layer which forms on this panel separates at the obstacle which the model forms. This three-dimensional separation becomes the "horseshoe" vortex center, but in the assymmetrical case which consists of a model at an angle of attack [10, 11] , it is especially the lower surface of of these vortexes which develops (Fig. 15b and A), and the separation line on the panel which continues to flow away from the model on the lower surface, very quickly turns back towards the socket on the upper surface (Fig. 17c);

- lastly, as has been observed many times on thick swept wings, the organized part on the upstream side of the marginal section enclosed by the main cone is the center of two secondary vortexes the first of which (T_1) moves along the separation line near the leading edge and turns in the same direction as the main

vortex T, whereas the second (T_2) moving in the opposite direction is inserted between these two vortexes (Fig. 15c, B and C). Under these conditions, the layer of flow which unrolls along the leading edge (Fig. 13c) divides into two substrata which feed the ma and the secondary vortices in the same direction respectively.

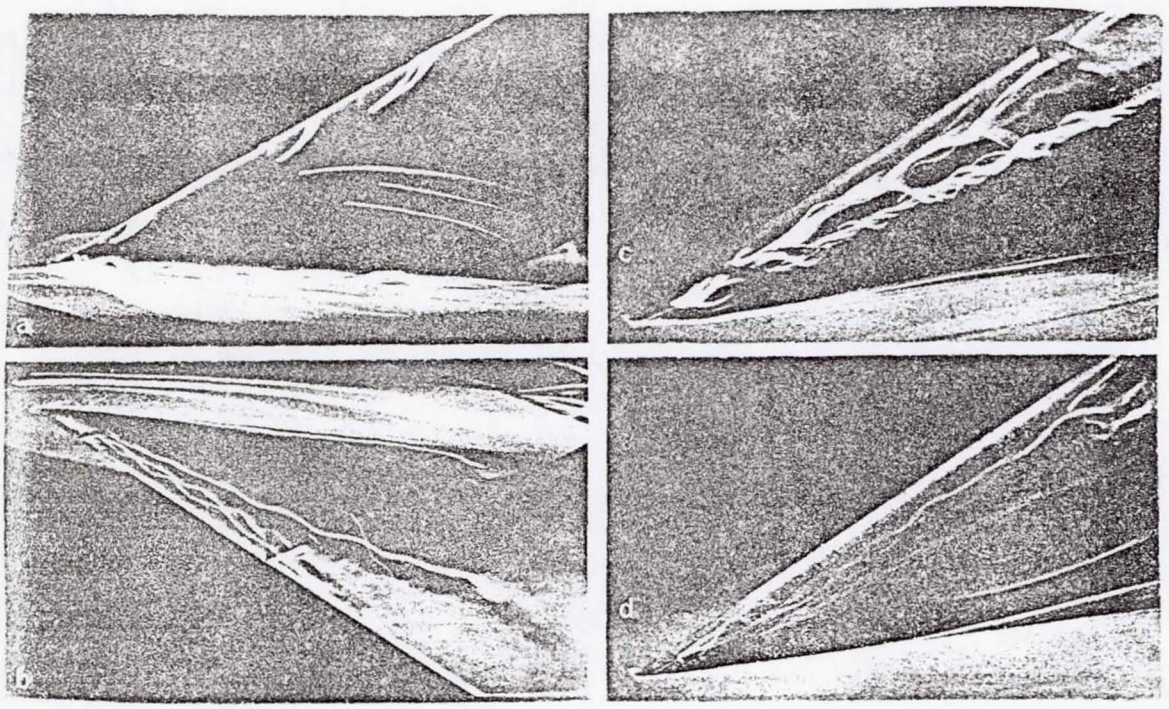

Fig. 13. - Flow around a model of an enlarged wing at a 20° angle of attack (water tunnel - $Re_c \simeq 10^4$). Views of the upper surface (b, c, d) and of the lower surface (a). /8

3.3. Effect of the Angle of Attack /10

The different views grouped in Figure 16 allow the course of the flow as a function of an increasing angle of attack α with constant $Re_c \approx 10^4$. With a small angle of attack (Fig. 16a') the lines of parietal current on the upper surface trail in the direction of the generating lines of the wing and only separate near the free end of the model.

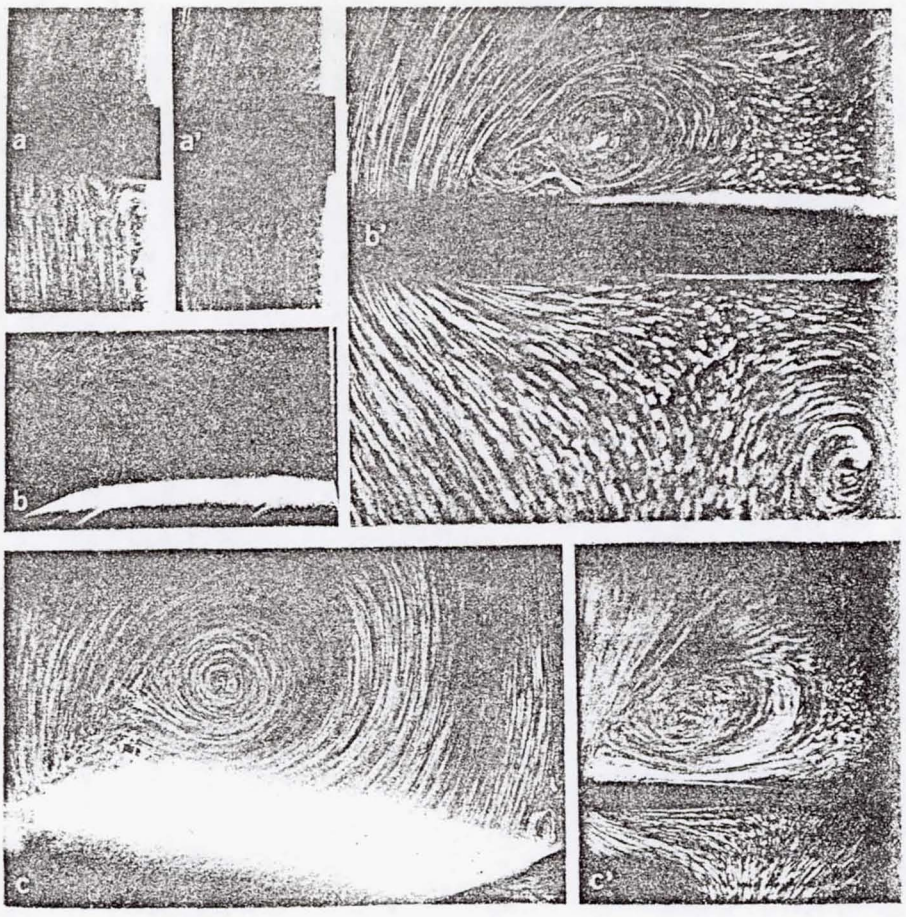

Fig. 14 - Flow around a model of an enlarged wing at a 20° angle of attack (water tunnel $Re_{\delta} \approx 10^4$). Cross-sections located near the apex (a, a'), in the mid-chord section (b, b') and upstream from the trailing edge (c, c') of the socket section according to Figure 11-2 (see note)
View following an axis parallel to the local tangent on the lower surface (a) or the upper surface (a'), at the vortex axis (b, c) or on the plane of the flying surface (b'. c').
Note: the section is located downstream from the breakdown point of the main vortex.

/9

With a 15° angle of attack (Fig. 16 b', b"), the separation /10 occurs along a generating line near the leading edge and it results from the formation of the vortex structure described above, with a well-organized main vortex from the apex near which its origin is located to the end of the model.

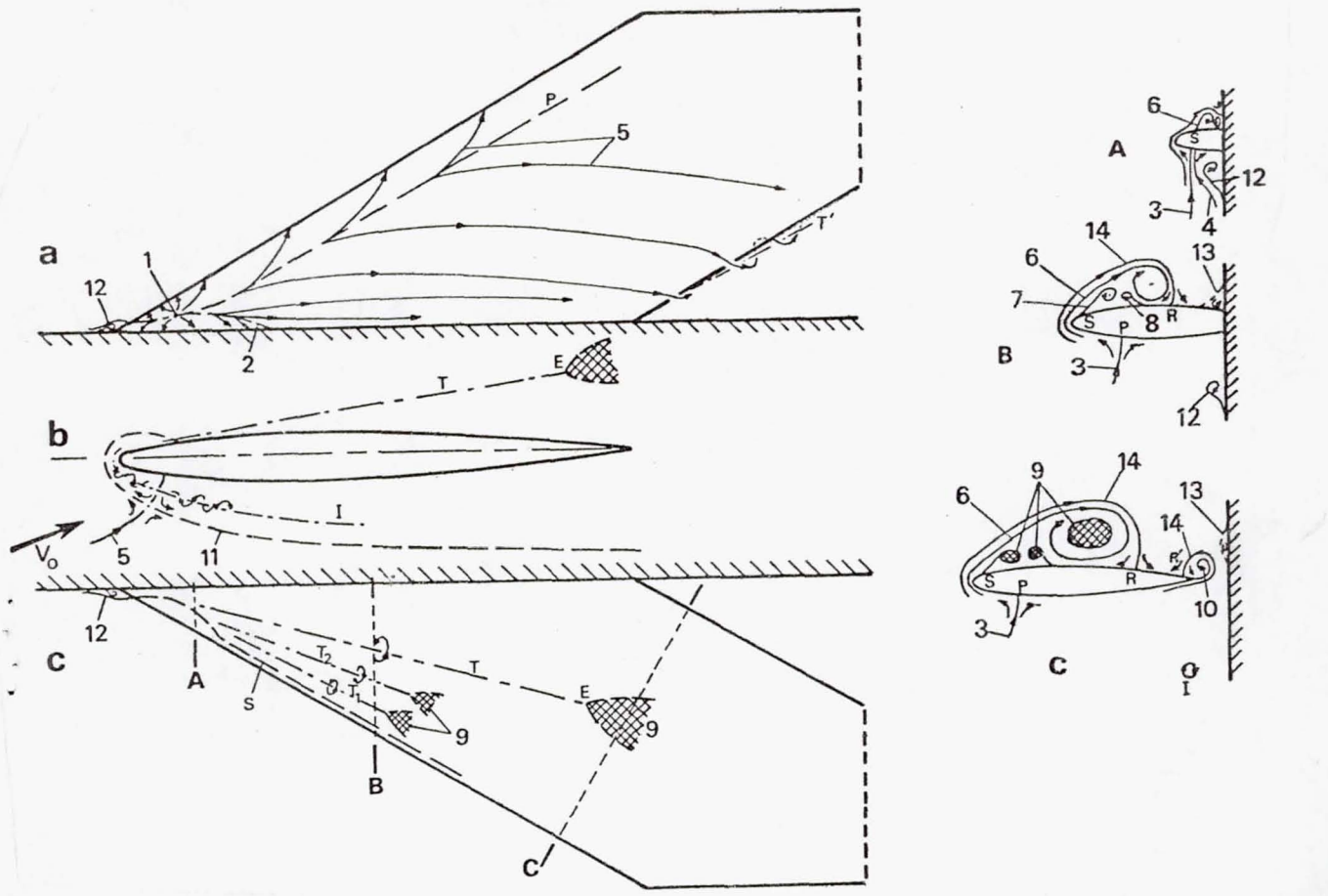

/10

Fig. 15 - Diagram of the flow around a cylindrical accentuated swept wing at high angle of attack. - a, b, c - diagrams relating to the lower surface, the socket and the upper surface. - A, B, C - diagrams of the transversal pseudo-flow at the top of the apex, of the mid-chord and downstream from the trailing edge of the socket section.

Key: 1. single nonisotropic stagnation point
P. } departure lines between the flows } the leading & trailing edges
2. } of the lower surface which are di- } the trailing edges and the
rected towards } protective panel
3 & 4. flow surfaces which end along lines P and 2.
5 parietal flow lines.
S main separation line on the upper surface
6 conical sheet winding around the main vortex T which breakdowns in E
7 & 8 secondary sheets winding around vortexes T_1 in the same direction and T_2 in the opposite direction of T
9 disorganized cores of vortexes T, T_1 and T_2
10 sheet twisted around the vortex at the trailing edge T'
11 separation line on the protective panel curved in on both sides of a departure point
12 sheet twisted around the main vortex I curved in the shape of a horseshoe and characterizing the separation on the panel

Fig. 15 continued

13 small separated regions observed on the protective panel
14 flow surfaces, boundaries of flow layers feeding the various vortexes on the upper surface and leading along the separation lines R and R'.

At an angle of attack of 20° (Fig. 16 c') and a fortiori at and angle of attack of 25° (Fig. 16d'd"), the vortex structure develops, the breakdown of the main vortex occurs on the downstream side and moves upstream, whereas the disorganization of the marginal sector progresses in the same direction.

While the separation line on the upper surface tends to be located more and more near the leading edge, the departure point on the lower surface moves further away as the angle of attack increases (Fig. 16 a b c d).

At an angle of attack of 25° , all of these phenomena are especially well developed: the visualizations then reveal the spiral structure of the breakdown of the main vortex (Fig. 17 d), and the shape curved in a horseshoe form of the vortexes on top of the apex and characterizing the separation of the boundary layer on the protective panel (Fig. 17 a b c). Due to a slit placed in the leading edge of the enlarged model of the apex and implemented in these tests, it was possible to emit a band of dye which directly visualizes a section of the vortex sheet which twists around the main vortex (Fig. 17c d). Likewise in order to allow a closer analysis of the three-dimensional separation on the protective panel and its course as a function of the angle of attack (Fig. 18), the dye was emitted along this flat wall in the form of a parietal sheet which passes around the separated region and isolated filaments of variable altitude, in other words more or less near this wall depending on the regulation of their flow, and which feed the horseshoe vortexes (Fig 17 b c) or become distorted before the separated band.

Figure 18 reveals the path as a function of an increasing angle of attack of the shape of this band near the apex in a laminar region (Fig. 18a - e) and moreover confirms that the appearance of

the phenomena does not change in a turbulent system such as that set in motion at $Re_c \approx 0.5 \times 10^5$ (compare Fig. 18 e e' e" and f f' f").

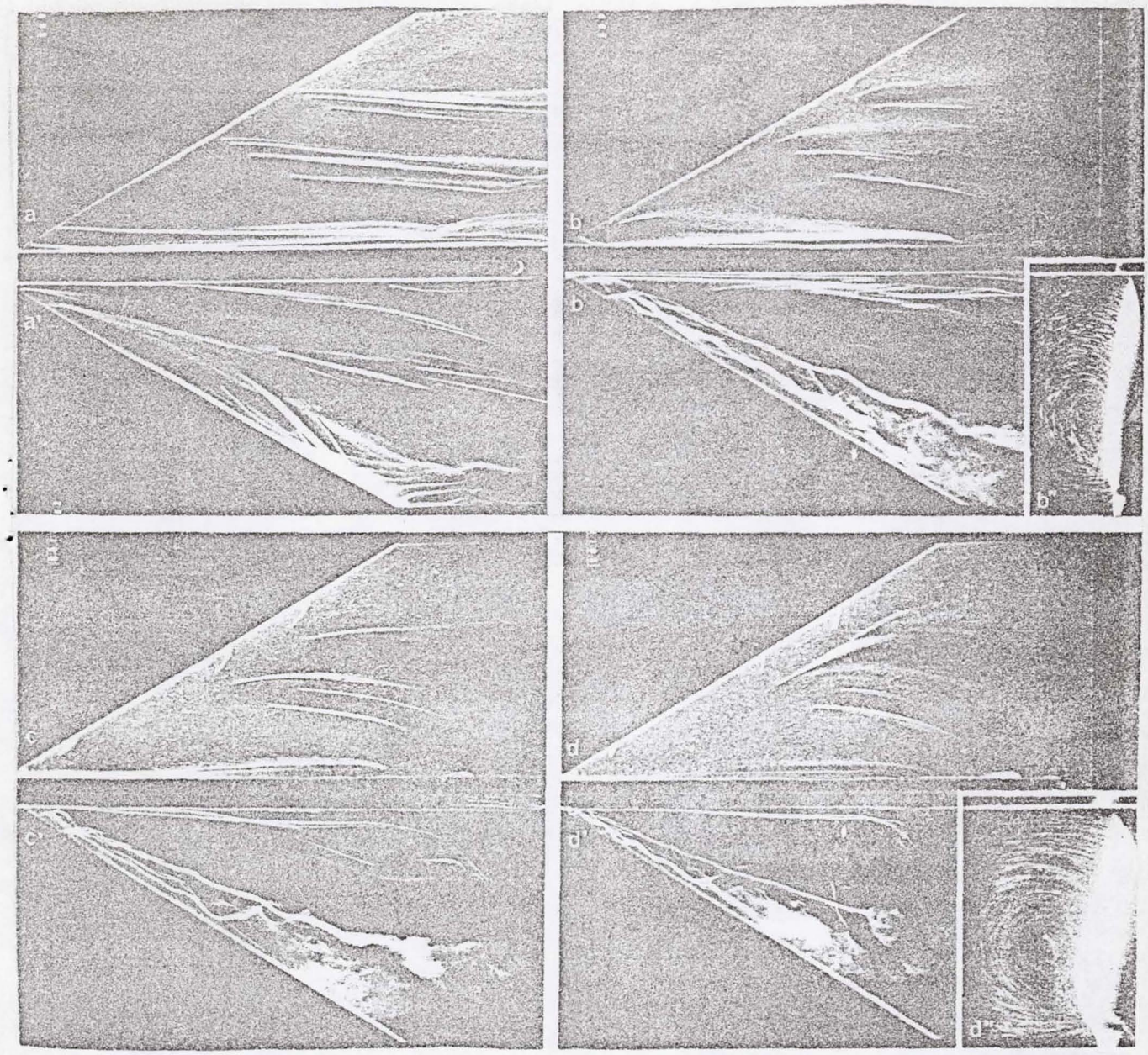

Fig. 16 - Effect of the angle of attack α on the flow around /11 an enlarged wing model (water tunnel - $Re_c \approx 10^4$). Views of the lower surface (a, c, c, d) and the upper surface (a', b', c', d') Cross-sections (b", d") downstream from the trailing edge of the socket section. $\alpha = 5°$ (a, a'), $\alpha = 15°$ (b, b', b"), $\alpha = 20°$ (c, c') and $\alpha = 25°$ (d, d', d").

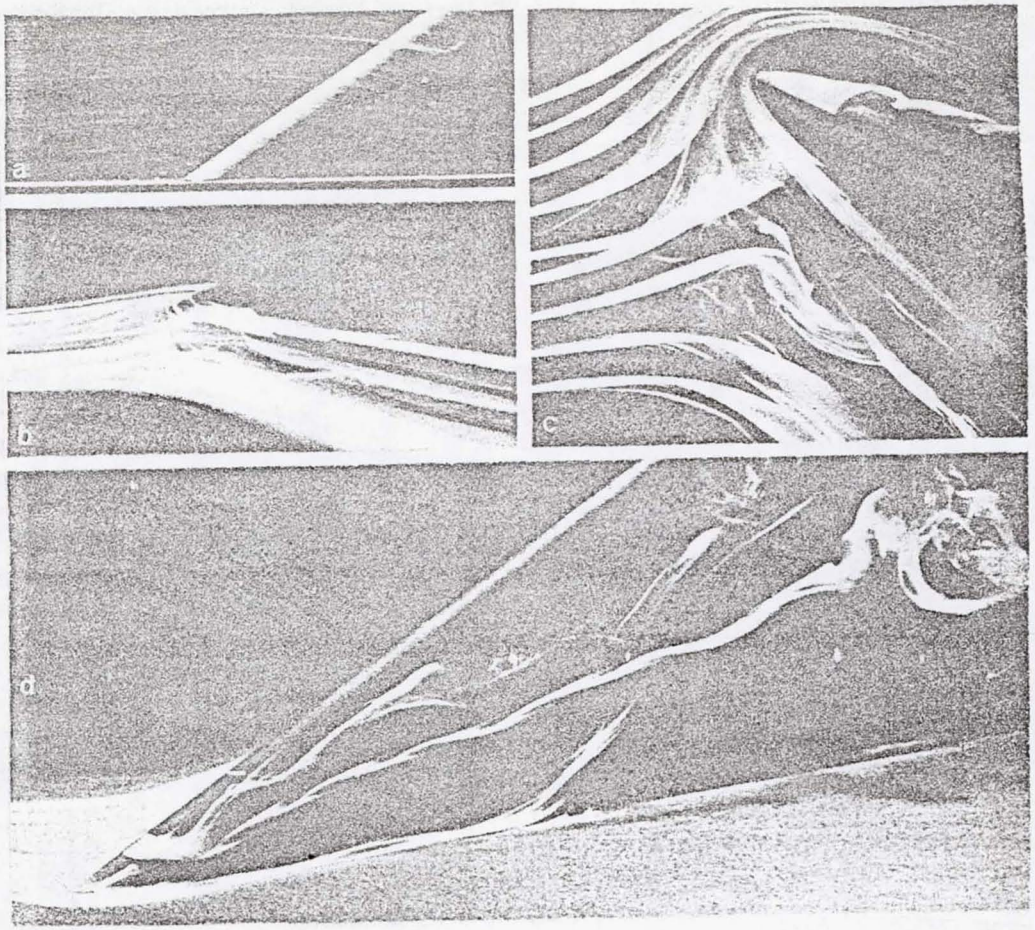

Fig. 17 - Flow around a model of an enlarged apex at a 25° angle of attack (water tunnel $Re_c \simeq 0.5 \times 10^4$). Views of the upper surface (d), of a wing section (c), of the lower surface (b), a longitudinal section passing through the apex (a) visualized by air bubbles. /12

4. Analysis in a Wind Tunnel of the Vortex Flow /13

In order to complete the information obtained at low Reynolds numbers, an exploratory study of the flow field on the upper surface of the wing was made in a wind tunnel on the following configuration: sweep $\phi = 60°$, angle of attack $\alpha = 19°$ corresponding to a Cz equal to 80% of the maximum Cz. This configuration shows a vortex separation involving almost all of the wing span and structured on the major part of its transversal dimension.

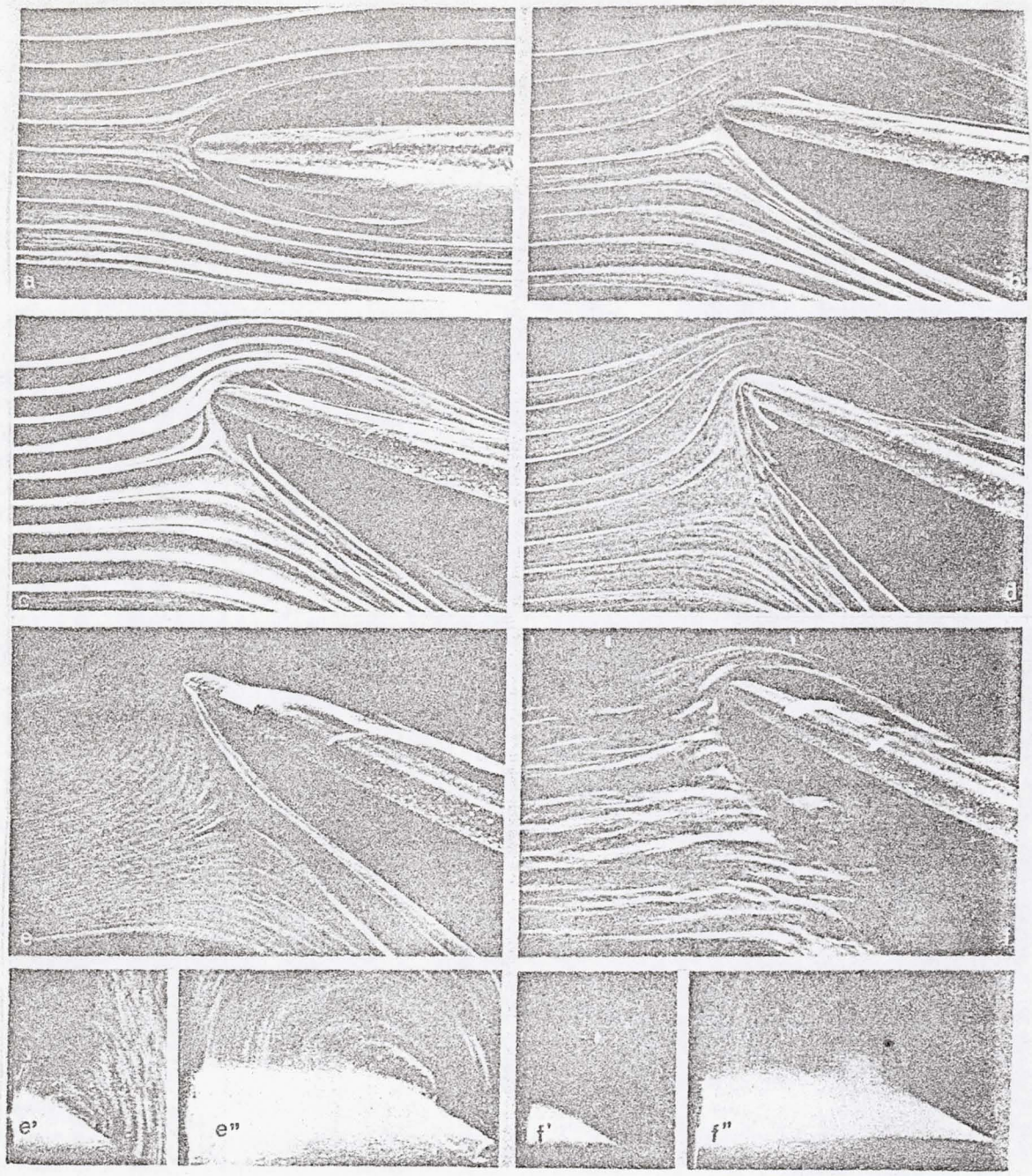

Fig. 18 - Effect of the angle of attack α and the Reynolds number Re_c on the flow along the protective panel and around an enlarged model of the apex (water tunnel - $Re_c \simeq 0.5 \times 10^4$) except when otherwise indicated.
$\alpha = 0°$ (a); $\alpha = 10°$ (b); $\alpha = 15°$ (c); $\alpha = 20°$ (d); $\alpha = 25°$ (e, e', e"); $\alpha = 25°$ with $Re_c \simeq 2 \times 10^4$ (f, f') (turbulent system).
Section views (a, b, c, d, e, f) - cross sections located near the apex (e', f') and the mid-chord (e", f") of the socket section.

The test speed of 90 m/sec ($Re_c = 1.9 \times 10^6$) ensures a rapid initiation of the transition especially when the flow separates.

4.1. General Flow Characteristics

The results of the probe normally made at the socket of the model in 6 sections, defined by the values of the abscissa x/c, are found in Figure 19. This representation of the pseudo-transversal flow reveals the extension and path of the vortex flow on the upper surface of the wing.

Near the apex (x/c = 0.24), the probe can only reach the outer part of the separation bubble whose thickness is very small. Moreover, we will note the effect of evident convolution near the leading edge.

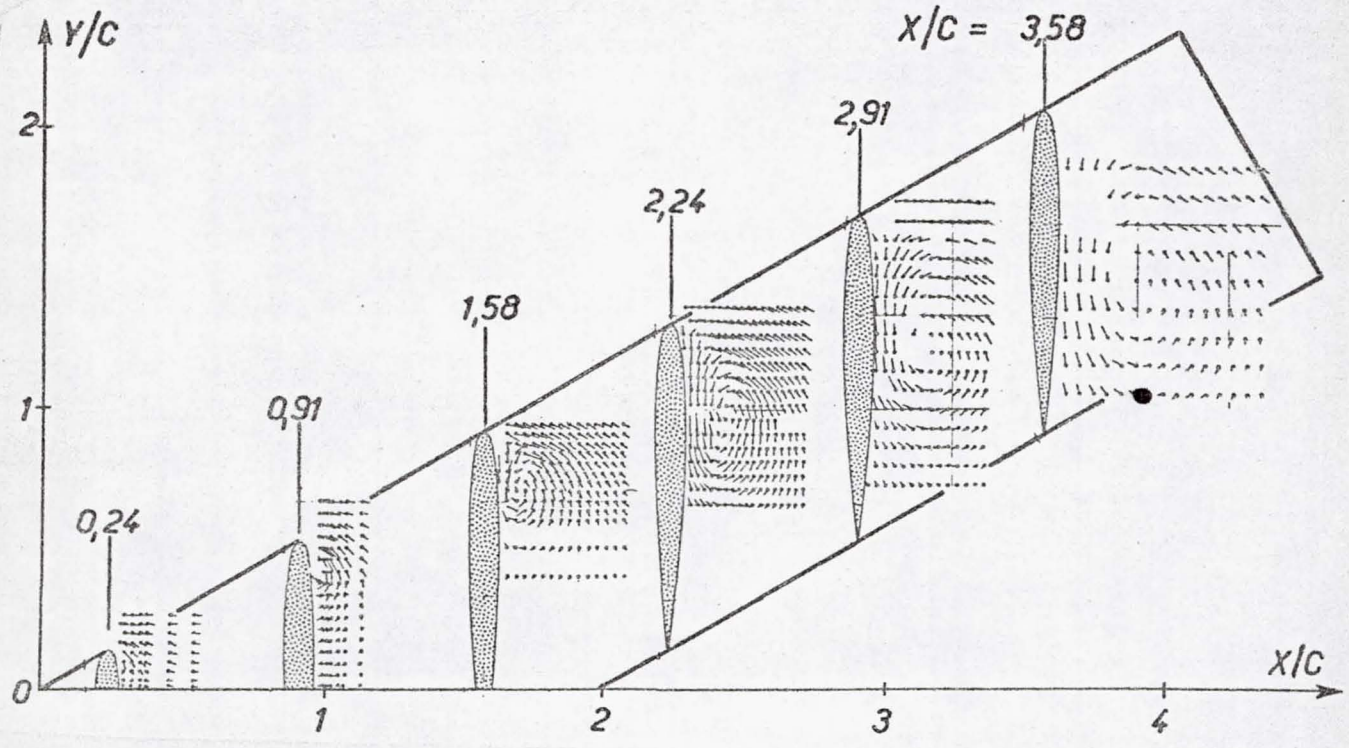

Fig. 19 - Projection of the Speed Vector on the Planes Which Are Probed /14

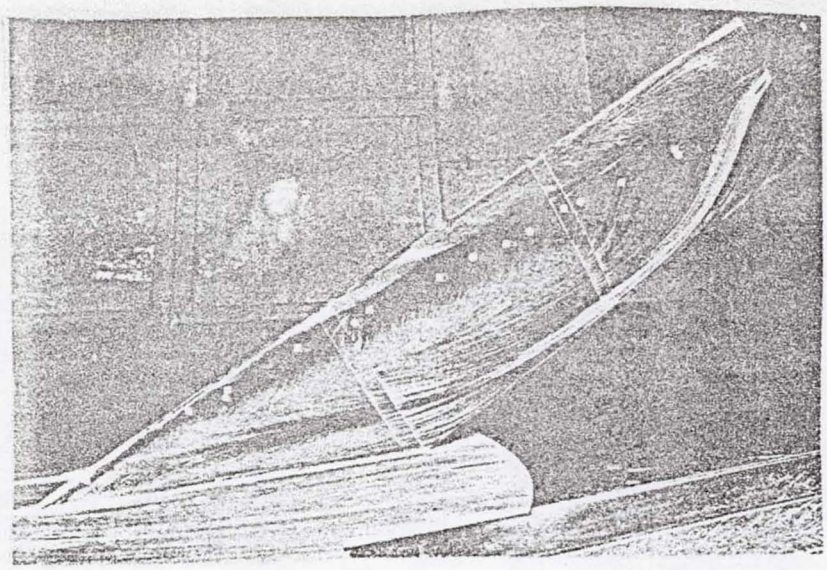

Fig. 20 - Visualization of Parietal Flow.
a) Positions of the vortex axis by probing O
b) Positions of the minimum parietal pressure □

For x/c = 0.91, a vortex structure is revealed. An evident /13
straightening of the flow direction at the level of the leading edge is associated to the formation of this structure. The region occupied by the upper surface vortex flow, already considerable starting at x/c = 1.58, then rapidly increases in size when x/c increases at the same time as the vortex axis moves away from the wing surface. The position of this axis, deduced from the probings, is given in Figure 21a in projection on the socket plane 0 zx and, in Figure 21b, in projection on the plane of chords Oxy. The latter plotting is transferred in Figure 20 onto the photograph of the parietal flow visualization as well as the position of the minimum pressure at the wall in various wing sections (see 2.2).

The comparison of these results indicates that the minimum pressure coincides with the projection on the plane of the chords of the main vortex axis and corresponds appreciably to the point of inflection of the parietal flow lines.

The change in the distance of the vortex axis from the wall shown in Figure 21a allows an initial region Σ_1 to be clearly distinguished, which slowly thickens and which corresponds to $x/c \leq 1$ of a central region Σ_2 where the vortex axis, considerably rectilinear, is much more inclined towards the wall ($\approx 5°$).

Lastly, we will observe that towards the end of the wing ($x/c \geq 3.58$) the vortex axis distinctly moves further and further away from the wall and tilts towards the socket (Fig. 21b) and tends towards a direction parallel to that of the general flow.

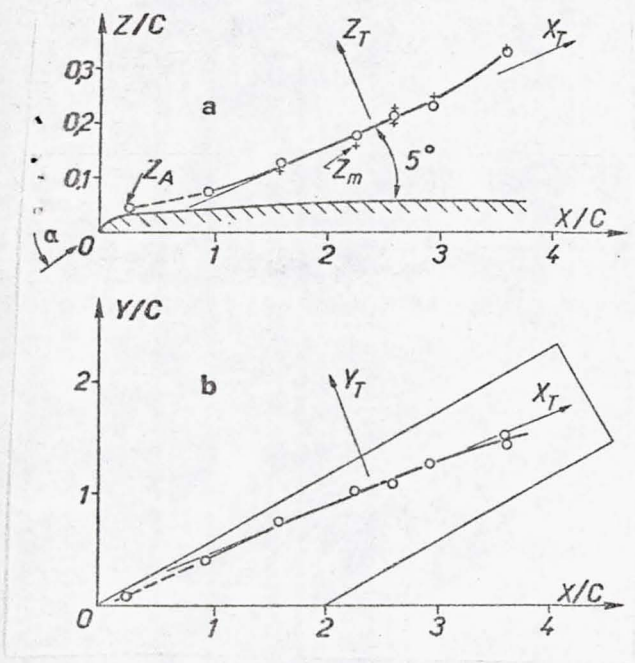

Fig. 21 - Position of the vortex axis by probing - a) in projection on the socket plane Oxz, b) in projection of the wing plane Oxy.

4.2. Formation of the Main Vortex - Study of the Initial Region Σ_1. /15

The probings obtained with the means defined in 2.1 only give limited information in the initial sections ($x/c \leq 1$) where the dissipative layers are not very thick. A detailed study of the parietal visualizations has thus attempted to specify the organization of this region of flow near the apex. Despite the inevitable role which interpretation plays in this procedure, this study completes, for a clearly higher Reynolds number value, the detailed observations obtained in the water tunnel (3.2).

First of all, it should be pointed out that the dissipative effects which are most obvious, characterizing the turbulent flow systems, tend to rapidly break up the small vortex structures, which could lead to a change in the organization of the secondary flows revealed in a laminar system. Figure 22 gives a detailed

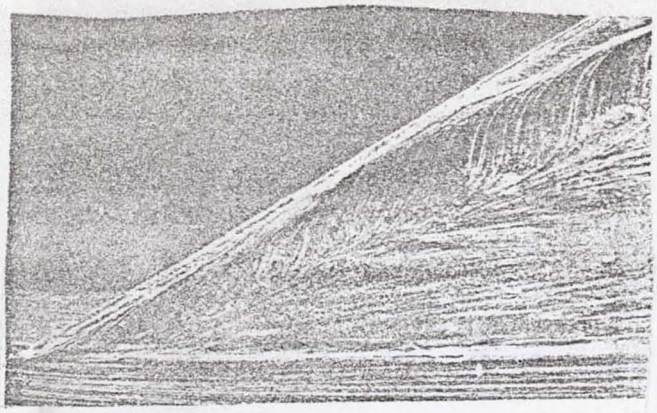

a.

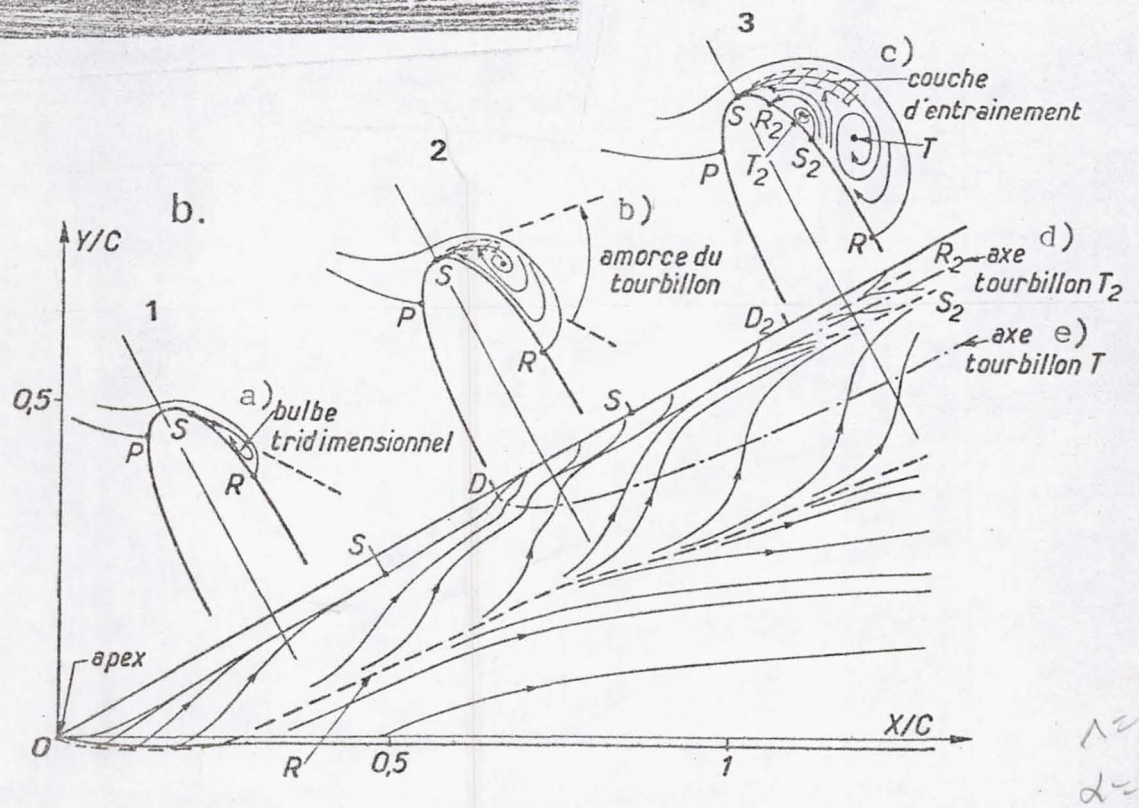

Fig. 22 - Details of the Flow in the Apex of the Wing Region
a) Parietal visualization
b) Diagram of the flow
Key for 22b: a) Three-dimensional bubble, b) starting vortex,
c) Driving line d) vortex axis T2,
e) vortex axis T

view of the parietal visualization obtained on the upper surface of the wing near the apex and the flow diagram which it suggests in which three regions can be distinguished:

- from 0 to D (Diagram 1) the flow coming from the lower surface moves around the leading edge and separates at S due to

the effect of the unfavorable pressure gradient which follows the leading edge overspeed. In this process, separation results from a considerable destabilization of the boundary layer and the the separated sheet hardly tilted towards the wall imprisons a very slow flow layer. The rejoining occurs along line R, considerably parallel to the leading edge separating the fluid which flows back from that moving downstream. The flow in the bubble thus formed is also fed along the socket by fluid coming from the protective panel, and flows transversely in a direction which is first of all continually changing and then which tends to become parallel to the leading edge.

- at point D, the visualization indicates a rapid rise of /16 the separation line towards the leading edge (Diagram 2, Fig. 22).

The phenomenon of non-convolution of the leading edge mainly due to the progressive increase in size of the local pseudo-angle of attack of the flow leading to a stall situation, causes a sudden straightening of the fluid sheet which separates, thus creating a circumstance favorable to the initiation of a coil characteristic of a conical vortex.

The parietal flow lines cause a very localized inflection downstream of point D which then spreads out and combines with the flow paths coming from the initial bubble to form a parietal path characteristic of a conical vortex structure (T).

Let us note that the re-attachment line R takes a direction which is tilted more downstream, a direction imposed by the development of the vortex (T). The flow confined between vortex T and the leading edge is pulled away by the fluid sheet at an accelerated speed which separates from the leading edge. It flows in a direction which becomes appreciably perpendicular to the latter. This configuration extends onto the part of the leading edge between points D and D_2.

- beyond D_2, the increase in transversal dimensions of vortex T leads to a change in the confined zone. A secondary separation S_2

occurs, followed by a readherence R_2 defining a small counter-vortex T_2 (Diagram 3, Fig. 22) which progresses along the leading edge with vortex T.

This description is basically the same for the results obtained in the water tunnel. It allows one to specify, when the laminar-turbulent transition occurs very near the separation, the effects caused by this circumstance on the organization of the flow near the apex.

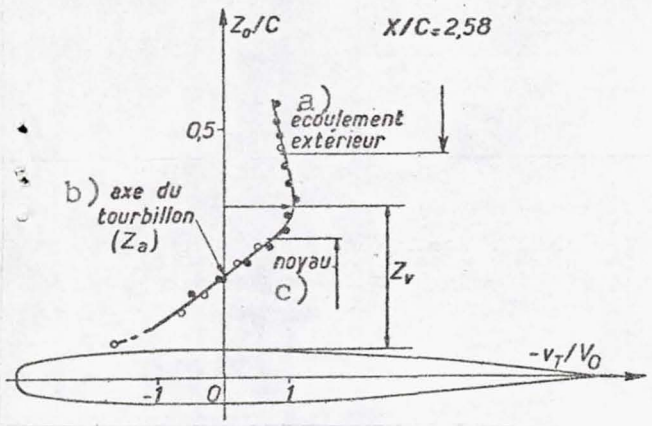

Fig. 23 - Change in the Speed Component $v_T(z_o)$.
Key: a) Exterior flow, b) Vortex axis, c) Core

4.3. Study of the Main Vortex T

In order to characterize the development of the vortex flow to its transition in each of the planes of exploration, the variation in the size of dynamic fields should be examined along axis z_o, perpendicular to the wing and passing through the center of vortex T. As an example, Figure 23 indicates the change in the component v_t of the speed from the transversal flow defined in the trihedral angle $ox_ry_rz_r$ linked to the vortex axis (See Fig. 21).

This diagram allows the core of the vortex which consists of a coil with perceptibly constant rotation to be distinguished from the exterior flow which does not rotate and to define the vortex center as well as a dimension z_v characteristic of its transversal dimension.

Figure 24 shows the change according to 2_o of the velocity modulus V/V_o for seven probing planes revealing a characteristic hollow on the z_m side which coincides considerably with the vortex axis (Fig. 21a).

The abscissa z_m of the maximum velocity also allows the transversal dimension of the vortex to be characterized. Moreover, it is very similar to the value z_v defined previously (see Fig. 25a).

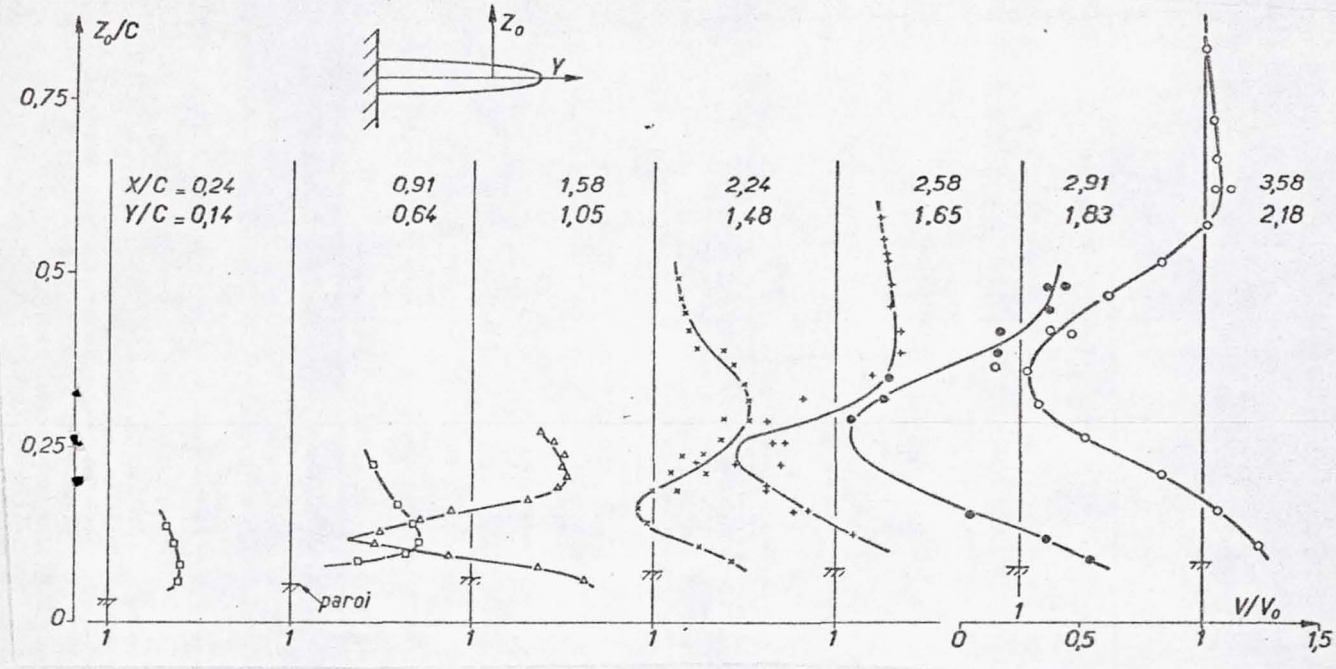

Fig. 24 - Change in Size of the Velocity Distributions $V(z_o)$.

In addition, we will note a sizeable dispersion of the measurements in certain sections, a dispersion which cannot be entirely attributed to an incorrect functioning of the probe submitted to too high angles of attack. The instability of the vortex structure which appears after $x/c \approx 2.24$ and which is especially evident for $x/c = 2.58$ is not to be dismissed. Moreover, it coincides with a change of system in the development of the vortex flow which we are now going to examine. /17

The longitudinal evolution of the vortex on the upper surface is thus characterized, at first analysis, by the three standard factors of its development: the transversal dimension z_v or z_m, the intensity of the vorticity of the core:

and the minimum velocity V_{min} on the axis. The evolution following x/c of these various dimensions is represented in Figure 25. Two distinct regions of evolution appear:

- for $x/c \leq 2.24$, an area of development where the minimum velocity on the axis increases while the transversal dimension of the vortex increases progressively with a correlative moderate decrease of the vorticity of the core.

- downstream from $x/c = 2.24$, an area where a sudden increase in the transversal dimension of the vortex is noted accompanied by a rapid decline of the vorticity and of the velocity on the axis. The origin of this area coincides with an evident instability of the vortex structure. This rapid evolution, caused by the slowing down of the general flow which the decrease in maximum velocity V_{max} measured at the boundary of the vortex indicates, defines the appearance of the process of breakdown of the vortex on the upper surface which seems to occur for $x/c > 3$.

5 Conclusion

The vortex flow on the upper surface of a wing having variable sweep placed at a high angle of attack was the subject of an in-depth experimental study in a wind tunnel and water tunnel. It was possible, by global efforts, to determine, as a function of the angles of attack and sweep, a field of existence of this type of flow which was then analyzed more closely by means of a static pressure field and parietal visualizations. An effect of the Reynolds number, especially on the angle of attack of the appearance of the vortex flow on this wing, could be observed.

The examination of the very structure of the separations which were organized around a conical vortex in a water tunnel with low Reynolds number resulted in the description of a very exact diagram of the vortex flow including its formation near the apex and its breakdown in the region of the trailing edge.

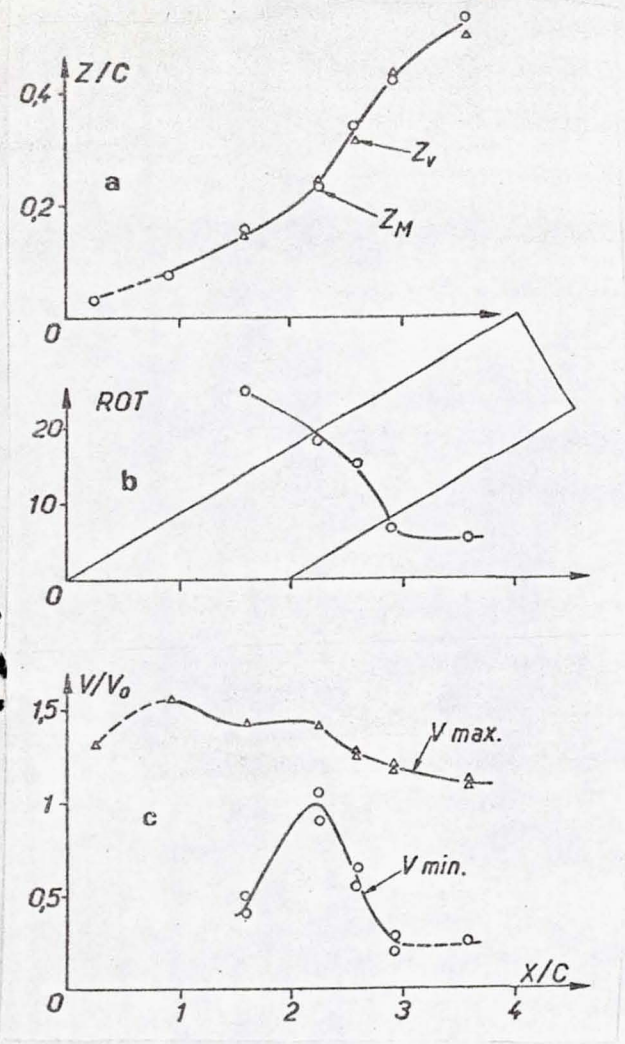

Fig. 25 - Longitudinal Evolution of the Vortex
a) transversal dimensions,
b) vorticity on the axis,
c) minimum and maximum velocities in the vortex.

This diagram proves to be rather similar to that which results from an analysis made in a wind tunnel with a much higher Reynolds number, involving the detailed scanning of the flow field on the upper surface of the wing as well as the parietal visualization for a special configuration.

In addition, these explorations allowed a detailed study of the evolution of the main vortex to be made and thus constitute a very valuable element in view of modelling such flows.

REFERENCES

1. Manie, F., Rehbach, C. and V. Schmitt, "Etude d'une aile à flèche variable en écoulement sub ou transsonique," [Study of a wing with variable sweep in sub or transsonic flow] ICAS Proceedings, Vol 2, Lisbon, 1978 (to be published).

2. Vincent, De Paul M. and A. Dyment, "Recherches sur les profils d'ailes en écoulement subsonique," [Research on Wing Sections in Subsonic Flow], L'Aeronautique et l'Astronautique, 19, 15-30 (1970-3).

3. El-Ramly, A.M. and W.S. Rainbird, "Computer-controlled system for the investigation of the flows behind wings," Journal of Aircraft, 14/7, 668-674 (1977).

4. Rebuffet, P., Aérodynamique expérimentale, Vol 2, Dunod, Paris 1966.

5. Werle, H., "Le tunnel hydrodynamique au service de la recherche aérospatiale"[The Water Tunnel Used in Aerospace Research] ONERA Publication 156 (1974).

6. Werle, H., "Ecoulements décollés," [Separated Flows] , AGARD Conference Proceedings No 168, Memoire No. 39, 1-14, 1975.

7. Roy, M., "Caractères de l'écoulement autour d'une aile en flèche accentuée," [Flow Characteristics About an Accentuated Swept Wing], CR Acad Sc. 234, 2501-2503 (1952).

8. Legendre, R., "Ecoulement au voisinage de la pointe avant d'une aile à forte flèche aux incidences moyennes," [Flow near the forward tip of a wing with high angle of sweep at average angles of attack], Recherche Aéronautique 30 (1952) and 31 (1953).

9. Werle, H., "Sur l'eclatement des tourbillons," [Vortex Breakdown] ONERA Technical Note No 175, 1971.

10. Young, A., "Some Special Boundary Layer Problems," Zeitschrift für Flugwissenschaften und Weltraumforschung 1 6, 401-414 (1977).

11. Hunt, J., Abell, C., Peterka, J. and H. Woo, "Kinematical Studies of the Flows Around Free or Surface Mounted Obstacles; Applying Topology to Flow Visualization," J. Fluid Mech. 86 Part I 179-200 (1978).

12. ONERA film No. 932 (1978): "Tourbillons sur une aile en flèche à grande incidence [Vortices on a Swept Wing at High Angle of Attack] (temporary silent version presented during the AGARD meeting in Sandefjord).